ELSEVIER

Journal of Chromatography A, 743 (1996) 221–229

JOURNAL OF CHROMATOGRAPHY A

Perfusion chromatography – characterization of column packings for chromatography of proteins

Mark McCoy*, Krishna Kalghatgi, Fred E. Regnier, Noubar Afeyan

PerSeptive Biosystems, Framingham, MA 01701, USA

Abstract

A Van Deemter equation modeling columns packed with spherical monodisperse perfusive media was utilized to calculate the predicted values of the effective pore diffusivity (D_p) and split ratio (α) of columns packed with POROS® and Oligo R3™ media. The validity of the model was established by calculating consistent values of D_p and α for lysozyme, α-chymotrypsinogen A and IgG using columns packed with POROS ion-exchange media. The split ratio was shown to be dependent on the pore structure of the media and not the eluite. The technique allows quantitative measurements of α and D_p, and is applicable for both perfusive and diffusive media.

Keywords: Stationary phases, LC; Proteins

1. Introduction

The significance of convective transport was first described in catalytic reaction engineering. A number of investigators have studied the flow profiles and effectiveness factors associated with intra-particle flow in catalyst particles. In 1973, Neale et al. [1] developed a model of creeping flow relative to an isolated permeable sphere and a swarm of permeable spheres. They concluded that intra-particle convection can have a significant effect on the settling velocity and overall permeability of a swarm of spheres. Nir and Pismen [2] developed a steady state model for heterogeneous catalysis in which the mass transport in porous catalysts occurred by concurrent intra-particle diffusion and convection coupled with a first order irreversible isothermal reaction. Convective transport was characterized by the intra-particle Peclet number ($\lambda=(v_p a)/D_p$). In addition, the authors provided estimates for particle permeability (K_p) and showed that a linear relationship existed between intra-particle flow (v_p) and superficial mobile phase velocity (V_f) at low Reynolds numbers. They also noted that intra-particle convection had little impact in systems restricted by a slow rate of reaction. Rodrigues and co-workers [3–8] reported a flow-rate dependence on D_p in large pore catalyst particles and attributed it to intra-particle convection. Modeling the particles as a one-dimensional slab, they determined the moments of an impulse of non-interacting tracer for fixed bed reactor. Applying moment analysis, the combined influence of intra-particle convection and diffusion were expressed as an apparent diffusivity (D) which varied with the intra-particle Peclet number. Further, they noted that concentration profiles within particles were asymmetric when convective flux through the particle became significant.

In 1989–1991, Afeyan and coworkers [9–11] introduced perfusion chromatography that takes advantage of intra-particle convection in adsorption chromatography and thus leads to enhancement of

*Corresponding author.

0021-9673/96/$15.00
PII S0021-9673(96)00371-8

chromatographic efficiency. POROS and Oligo R3 represent families of column packings derived from cross-linked polystyrene–divinylbenzene matrix with appropriate surface modifications for chromatography of biopolymers. The POROS particles used in these studies had unique pore structure that allows intra-particle convection in throughpores (d_{pore}> 5000 Å). The high surface area necessary for adequate sample capacity was achieved by a network of smaller size pores (300 Å<d_{pore}<700 Å) branching from the throughpores. POROS 1, Fig. 1a, has been developed to maximize intra-particle convection. Oligo R3, Fig. 1b, has been developed to maximize surface area. The design criterion of POROS 2, Fig. 1c, falls between that of POROS 1 and Oligo R3. The surface area of POROS 2 is greater than that of POROS 1 but less than that of Oligo R3.

Perfusion Chromatography® was modeled for both frontal [12–16] and zonal [17–22] modes. These models included the effects of axial dispersion, external diffusion (film mass transfer), intra-particle diffusion, intra-particle convection and interaction at the chromatographic surface. Perfusive supports were modeled as monodisperse or bidisperse slabs, or bidisperse spheres. As the mobile phase velocity increased, perfusive media exhibited significant enhancement in column efficiency and dynamic over conventional diffusive media.

The central purpose of the research summarized in this paper is to use established models of linear, perfusion chromatography to measure the intra-par-

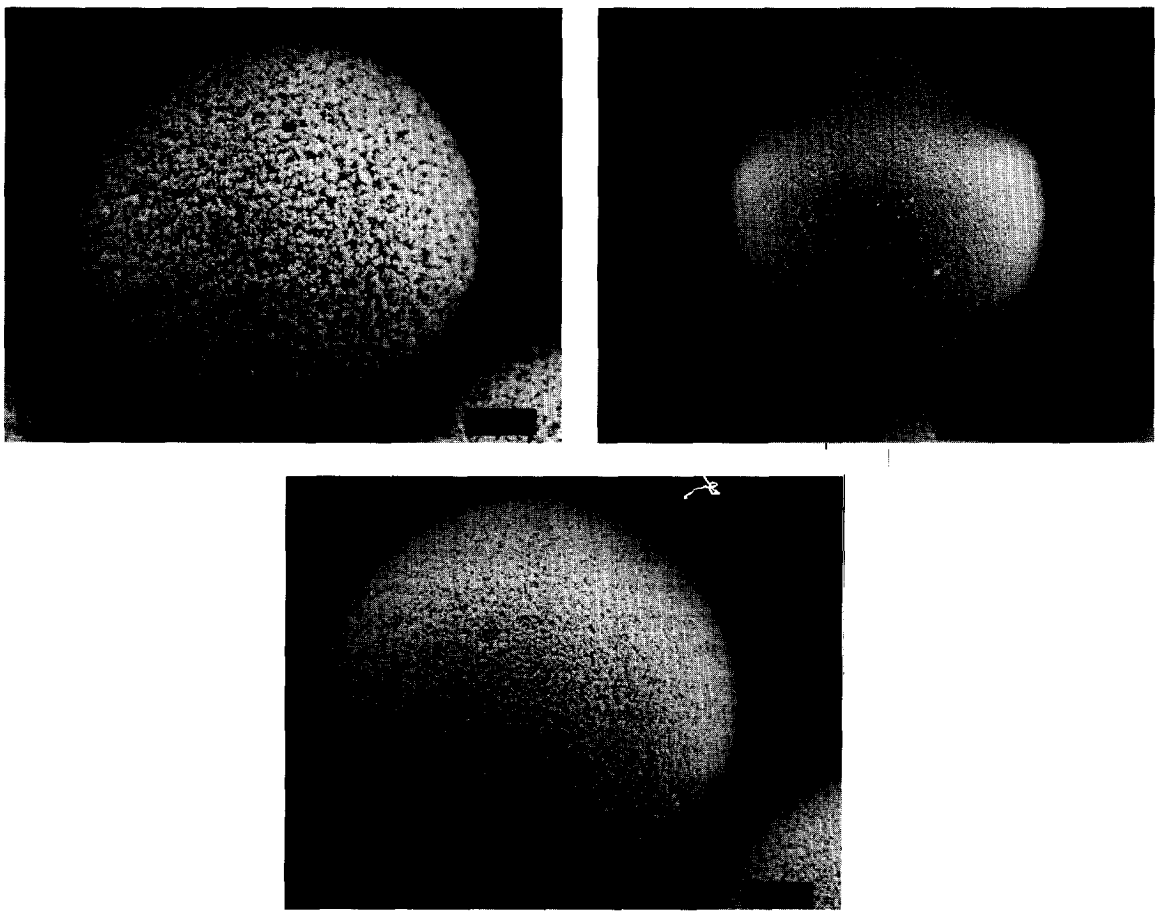

Fig. 1. Scanning Electron Micrographs. (a) POROS 1. Media: POROS 50 R1, Magnification ca. 975×. (b) Media: Oligo R3, Magnification ca. 975×. (c) POROS 2. Media: POROS 50 R2, Magnification ca. 975×.

ticle mass transport of POROS 1, POROS 2 and Oligo R3. Intra-particle mass transport can be characterized by the effective pore diffusivity and the volumetric ratio of mobile phase passing through the media to that passing around the media, i.e., the split ratio. To achieve this characterization, a chromatography model relating the HETP (H) to the effective pore diffusivity (D_p) and split ratio (α) will be presented. Using non-linear regression D_p and α will be calculated from experimental Van Deemter curves.

2. Theory

Perfusion chromatography was modeled following the approaches described previously for columns packed with diffusive, monodisperse spheres [23,24]. By using a monodisperse model, it is assumed that the diffusional resistance in the network of smaller size pores (300 Å$<d_{pore}<$700 Å) branching from the throughpores does not substantially contribute to the overall mass transfer resistance. In these studies, the effects of axial dispersion, external diffusion (film mass transfer), intra-particle diffusion and adsorption from the stagnant mobile phase inside the pores onto the interactive regions of the matrix were examined. It was assumed that the mobile phase was incompressible and isothermal conditions prevailed. The model is applicable for dilute eluite concentrations where the mobile phase flow-rate is not influenced by adsorption of the eluites. The Van Deemter equation [25] was derived from the moments of the column material balances:

$$H = \frac{\sigma^2}{\mu^2} L_o = \frac{2\varepsilon D_L}{V_f} + (C_{kf} + C_{Dp} + C_{kl})V_f \qquad (1)$$

Here, ε is the interstitial void fraction, D_L is the axial dispersion coefficient, V_f is the superficial velocity of the mobile phase, μ is the mean of the eluite residence time distribution (first absolute moment), and σ^2 is the variance of the eluite residence time distribution (second central moment). The C term is expressed in individual terms; C_{kf}, C_{Dp} and C_{kl}, for external diffusion (film mass transfer), intra-particle diffusion and adsorption, respectively.

Since the liquid flows through and around perfusion particles, the external contiguous boundary layer is absent. Film mass transfer is not relevant, hence the term C_{kf} in Eq. 1 can be eliminated. Under unretained conditions C_{kl} reduces to zero. Expanding C_{Dp} [23,24], Eq. 1 yields,

$$H = \frac{2\varepsilon D_L}{V_f} + \frac{2(1-\varepsilon)\varepsilon_p(1+K)^2 R_p^2/(15D_p)}{(\varepsilon + (1-\varepsilon)\varepsilon_p(1+K))^2} V_f \qquad (2)$$

where D_p is the effective pore diffusivity, R_p is the radius of the media, ε is the interstitial void fraction, ε_p is the particle porosity, and K is the Henry's law constant ($K=0$ for an unretained adsorbate). At high mobile phase velocities ($2\varepsilon D_L/V_f \rightarrow 0$), Eq. 2 predicts a linear relationship between H and V_f, with the slope of the Van Deemter curves proportional to R_p^2/D_p.

Eq. 2 is modified to incorporate intra-particle convection by addition of the convective enhancement factor $f(\lambda)$ developed for spherical particles [5,21],

$$f(\lambda) = \left(\frac{3}{\lambda}\left[\frac{1}{\tanh(\lambda)} - \frac{1}{\lambda}\right]\right) \qquad (3)$$

where λ is the intra-particle Peclet number. The general form of λ was defined in Nir and Pismen [2] as,

$$\lambda = \frac{v_p a}{D_p} \qquad (4)$$

where a is the characteristic dimension of the perfusive particle, v_p is the intra-particle velocity and D_p is the effective pore diffusivity. The particle diameter (d_p) [10], particle radius (R_p) [9], and one-third of the particle radius ($R_p/3$) [5,21] all have been utilized previously as the characteristic particle dimension. Irrespective of which characteristic dimension is utilized the information conveyed in λ is unchanged. The Peclet number employed in this article is based on the characteristic particle dimension of $R_p/3$. Thus,

$$\lambda = \frac{v_p(R_p/3)}{D_p} \qquad (4a)$$

The enhancement factor lumps the effects of intra-particle convection and diffusion into the apparent diffusivity, D_p^a,

$$D_p^a = \frac{D_p}{f(\lambda)} \tag{5}$$

Replacement of D_p in Eq. 2 by D_p^a yields a Van Deemter equation which incorporates intra-particle diffusion and convection.

$$H = \frac{2\varepsilon D_L}{V_f} + \frac{2(1-\varepsilon)\varepsilon_p(1+K)^2 R_p^2 f(\lambda)/(15D_p)}{(\varepsilon + (1-\varepsilon)\varepsilon_p(1+K))^2} V_f \tag{6}$$

The intra-particle velocity (v_p) is related to V_f via the split ratio,

$$v_p = \frac{\alpha}{(1-\varepsilon)\varepsilon_p} V_f \tag{7}$$

The split ratio (α) is the volume fraction of mobile phase flowing through the media.

The particle permeability (K_p) can be calculated using the Blake-Kozeny equation [26].

$$K_p = \frac{\varepsilon_p^3}{150(1-\varepsilon_p)^2} d_m^2 \tag{8}$$

Afeyan et al. [9] modeled POROS particles as an agglomerate of spherical micro-particles fused together into a continuous structure. According to these studies, the particle porosity (ε_p) and the micro-particle diameter (d_m) for POROS media were in the order of 0.6 and 1.0 μm, respectively. With these values in mind, the permeability of these particles (K_p) will be on the order of 9×10^{-11} cm^2 and the total bed permeability (K) will approach that of a bed packed with impermeable spheres [1]. This supports the assumption in [9] that the pressure drop over the column is due to interstitial flow and leads to the following expression for the split ratio.

$$\alpha = \frac{K_p}{K}(1-\varepsilon)^2 \tag{9}$$

The split ratio will be constant for a well-packed column containing rigid media making it a suitable measure of intra-particle convection.

Two asymptotic cases are described. As V_f approaches zero, Eq. 7 indicates that λ will approach zero. By applying the limit,

$$\lim_{\lambda\to 0} f(\lambda) = 1 \tag{10}$$

Eq. 6 reduces to Eq. 2, a Van Deemter equation for purely diffusive media. Thus, at low flow velocities convective enhancement is negligible and diffusion is the dominant mode of the intra-particle mass transport. The Van Deemter curve of a column packed with perfusive media approaches a linear asymptote in this region.

At high V_f, the intra-particle Peclet number becomes large. By applying the limit,

$$\lim_{\lambda\to\infty} f(\lambda) = \frac{3}{\lambda} = \frac{9D_p(1-\varepsilon)\varepsilon_p}{\alpha V_f R_p} \tag{11}$$

Eq. (6) reduces to

$$H = \frac{2\varepsilon D_L}{V_f} + \frac{2(1-\varepsilon)\varepsilon_p(1+K)^2 R_p(3/5)(1-\varepsilon)\varepsilon_p/\alpha}{(\varepsilon + (1-\varepsilon)\varepsilon_p(1+K))^2} \tag{12}$$

Thus, convection dominates intra-particle mass transfer at high values of λ. At this limit H is proportional to R_p/α and is independent of V_f and D_p. This asymptotic behavior is applicable to the monodisperse particle model. A bidisperse model does not predict an H independent of V_f at high values of λ.

In summary, Eq. 6 is applicable for all values of λ, viz. (a) the diffusive region ($\lambda\to0$), (b) the transition region where both intra-particle diffusive and convective are significant and (c) the region of convective dominance ($\lambda\to\infty$).

3. Experimental

3.1. Materials

High-performance liquid chromatography (HPLC) grade acetonitrile (ACN) and reagent grade trifluoroacetic acid (TFA) were obtained from J.T. Baker (Phillipsburgh, NJ, USA). Insulin, IgG, lysozyme, α-chymotrypsinogen A, buffers and inorganic salts were obtained from Sigma (St. Louis, MO, USA). Aqueous solutions were prepared using HPLC grade water (J.T. Baker) and filtered through a 0.45 μm filter (VWR Scientific, Boston, MA, USA). The

eluents were degassed by sonication while applying vacuum.

3.2. Instrumentation and columns

The experiments were performed using a BioCAD™ Workstation (PerSeptive Biosystems, Framingham, MA, USA). The instrument includes an integrated UV–Vis detector which was equipped with a 4.5 μl flow cell having a path length of 3 mm. The instrument delivers precise flow-rates up to 20 ml/min. Actual flow-rates were measured for each experimental setting. POROS and Oligo R3 media were from PerSeptive Biosystems.

The media was slurry packed into PEEK column hardware (100×4.6 mm) and held in place using 2 μm frits. Column efficiency and peak symmetry were determined at 180 cm/h using a small molecular weight probe ($NaNO_3$ for ion-exchange media and acetone for reversed-phase media) under unretained conditions. Column and media specifications are listed in Table 1.

The scanning electron micrographs were taken with the Topcon model 510 Scanning Electron Microscope (Topcon, Tokyo, Japan).

3.3. Procedure

All experiments were conducted under non-retained conditions. The delay volume was measured using a low-molecular-mass probe with a zero dead volume union in place of the column. Short segments of small diameter (0.125 mm) tubing were used to minimize the extra-column effects. The eluite concentration was 1.0 mg/ml for all proteins. A fixed amount of the sample between 1 and 10 μl was used for each experimentally measured Van Deemter curve. This ensured that the peak heights of the eluites ranged from 0.3 to 0.7 AU. Absorbance was measured at 215 nm. The column and the eluents were maintained at constant temperature using a column oven and by placing the eluent reservoirs in a circulating water bath. The retention data were corrected for the delay volume.

3.4. Parameter regression

Predicted values of the effective pore diffusivity and split ratio were calculated by minimizing the sum square error (*SSE*) between the experimental theoretical plate height (H_i) and values of predicted theoretical plate height ($\hat{H}_i$) calculated from Eq. 6.

$$SSE = \sum_{i=1}^{n} (H_i - \hat{H}_i)^2 \tag{13}$$

The axial dispersion coefficient (D_L) was calculated using a correlation obtained from Gunn [27]. The bed porosity (ε) was taken as 0.35 [28]. The values of H_i were calculated by the BioCAD software according to the formulas,

$$N = 2\pi\left(\frac{h' t_r}{A}\right)^2 \tag{14}$$

and

$$H = \frac{L_o}{N} \tag{15}$$

Table 1
List of column packings and specifications.The efficiency (N) was determined using 100×4.6 mm columns for small molecular probes ($NaNO_3$ for ion-exchange or acetone for reversed-phase) under unretained conditions. The terms d_p, N and b/a represent particle diameter, the theoretical plates per meter and asymmetry ratio measured at 10% of the peak height

Media	Name	Class	(d_p) (μm)	Efficiency (N/m)	b/a
Reversed-phase	POROS 20 R1	POROS 1	20	18 600	0.9
	POROS 20 R2	POROS 2	20	11 200	1.2
	Oligo R3	Oligo R3	30	10 000	1.1
	POROS 50 R1	POROS 1	50	4400	1.1
	POROS 50 R2	POROS 2	50	5900	1.0
Ion-exchange	POROS 20 SP	POROS 1	20	13 010	1.1
	POROS 20 HQ	POROS 1	20	9403	1.1

where N is the number of theoretical plates, t_r is the retention time, h' is the peak height, A is the peak area and L_o is the length of the column.

4. Results and discussion

4.1. Pore diffusivity and flow split ratio

The proposed model was validated by experiments carried out using columns packed with POROS 20 SP and POROS 20 HQ media. These are POROS 1 media and exhibit a pore structure that allows relatively high intra-particle convection. The Van Deemter plots for insulin, α-chymotrypsinogen A and IgG obtained for a POROS 20 SP column are shown in Fig. 2. Similar plots for lysozyme, α-chymotrypsinogen A and IgG obtained for a POROS 20 HQ are shown in Fig. 3. Results are summarized in Table 2 for POROS 20 SP and POROS 20 HQ. The column packed with POROS 20 SP yielded similar predictions of the split ratio for each of the eluites. This agrees with Eq. 9 that predicts a to be invariant of the nature of the eluite. Comparable results were obtained for the column packed with POROS 20 HQ.

For both columns, the Van Deemter curves for lysozyme, insulin and α-chymotrypsinogen A remained in a transition region, their slopes were decreasing at the upper range of V_f. Under these conditions, resistance due to intra-particle diffusion was substantially reduced by intra-particle convection, but its effects were not completely eliminated. At high values of V_f, the plate heights of IgG were constant, indicative of convective dominant intra-particle mass transport (Eq. 12). The consistent values of the split ratio obtained from these ex-

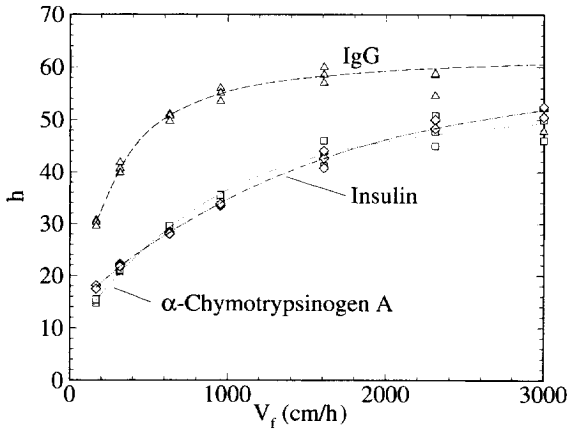

Fig. 2. Van Deemter plots for POROS 20 SP. Column: 100×4.6 mm. Eluent: 50 mM sodium phosphate buffer containing 0.5 M NaCl, pH 7.0. $k'=0.0$ and temp. = 20°C. (□) α-Chymotrypsinogen A (exp.), (△) IgG (exp.), (◇) insulin (exp.), (····) α-chymotrypsinogen A (prediction), (—) IgG (prediction), (-·-·) insulin (prediction).

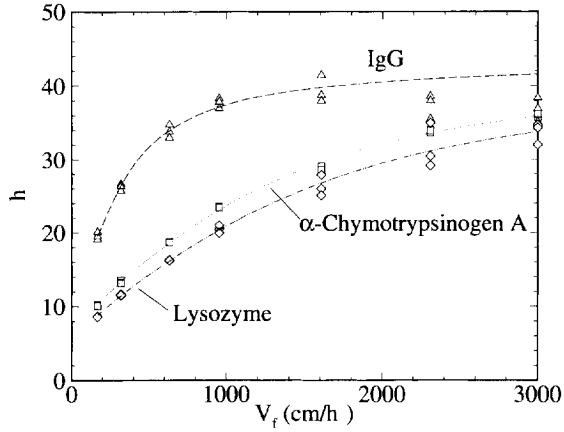

Fig. 3. Van Deemter plots for POROS 20 HQ. Column: 100×4.6 mm. Eluent: 50 mM Tris–HCl buffer, 0.5 M NaCl, pH 8.5. $k'=0.0$ and temp. = 20°C. (□) α-Chymotrypsinogen A (exp.), (△) IgG (exp.), (◇) lysozyme (exp.), (····) α-Chymotrypsinogen A (prediction), (—) IgG (prediction), (-·-·) lysozyme (prediction).

Table 2
The predicted values of tortuosity (τ) and split ratios (α) for POROS 20 SP and POROS 20 HQ determined by non-linear regression (Section 3.4). The experimental conditions are as given under Fig. 2 for POROS 20 SP and under Fig. 3 for POROS 20 HQ. The values of free molecular diffusivity (D) of proteins were taken from literature [29]

Protein	$D\times10^{11}$ (m^2/s)	τ	$\alpha\times100$
POROS 20 SP			
Insulin	13.7	1.7	0.37
α-Chymotrypsinogen A	9.5	1.9	0.40
IgG	4.0	2.3	0.35
POROS 20 HQ			
Lysozyme	11.2	1.1	0.49
α-Chymotrypsinogen A	9.5	1.0	0.50
IgG	4.0	1.5	0.53

perimental Van Deemter curves indicate that Eq. 6 is an adequate model for the media studied.

The tortuosity factors (τ) for POROS HQ 20 and POROS SP 20 media were estimated from the predicted values of D_p and literature values of free molecular diffusivity of the eluites [29]. These values were in good agreement for each column as shown in Table 2. At low V_f, the slopes of Van Deemter curves were inversely proportional to D_p, an indication that mass transfer in this region is dominated by intra-particle diffusion.

Another class of perfusive media designated as POROS 2, was developed with a greater accessible area for molecular interaction while maintaining its perfusive characteristics. In comparison to POROS 1, these particles were designed to have a lower fraction of the throughpores and increased capacity. The predicted values of split ratios of the reversed-phase media employed in this study were determined using lysozyme as a probe, under non-retained conditions. The Van Deemter curves are shown in Figs. 4 and 5. The results are summarized in Table 3. As expected, the split ratios of POROS R2 (20 and 50 μm) particles were found to be 3 to 4 times lower than those of POROS R1 (20 and 50 μm) media.

Oligo R3 is a reversed-phase packing with a mean

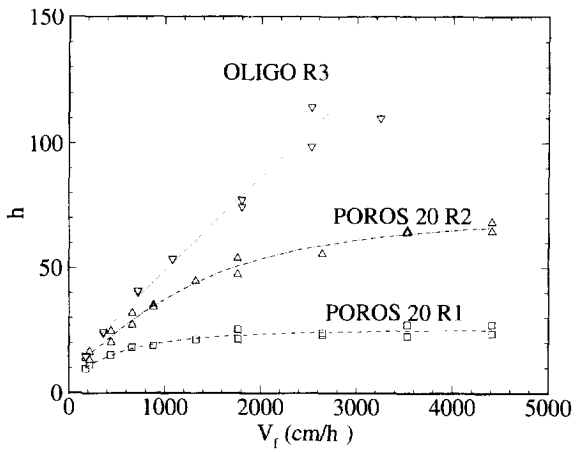

Fig. 4. Van Deemter plots for POROS 20 μm reversed-phases using lysozyme. Column: 100×4.6 mm. Eluent: 50% (v/v) ACN in water containing 0.1% TFA. $k'=0.0$ and temp.=30°C. (□) POROS 20 R1 (exp.), (△) POROS 20 R2 (exp.), (▽) Oligo R3 (exp.), (—) POROS 20 R1 (prediction), (- - -) POROS 20 R2 (prediction), (· · · ·) Oligo R3 (prediction).

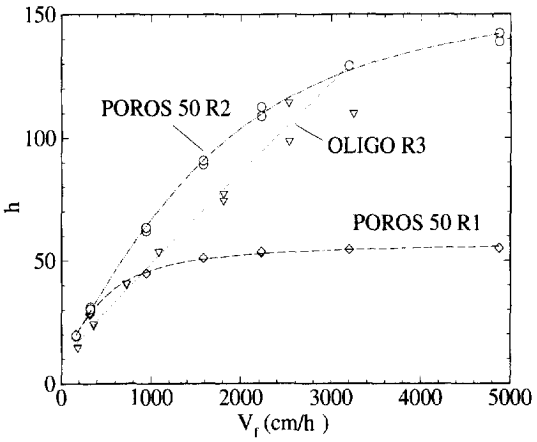

Fig. 5. Van Deemter plots for POROS 50 μm reversed-phases using lysozyme. Column: 100×4.6 mm. Eluent: 50% (v/v) ACN in water containing 0.1% TFA. $k'=0.0$ and temp.=30°C. (◇) POROS 50 R1 (exp.), (○) POROS 50 R2 (exp.), (▽) Oligo R3 (exp.), (—) POROS 50 R1 (prediction), (- - -) POROS 50 R2 (prediction), (· · · ·) Oligo R3 (prediction).

diameter of 30 mm and was designed to maximize the area accessible to molecular interaction. The Van Deemter curve of Oligo R3 was linear. The predicted value of split ratio for Oligo R3 was calculated in the same manner as for POROS 20 and POROS 50 media, i.e., both α and D_p were allowed to regress. Even then, the predicted value of α was zero. The results summarized in Table 3 strongly suggest that Oligo R3 is a diffusive support.

In contrast to purely diffusive media that exhibit linear relationships between H with V_f, the slope of the Van Deemter curves for POROS media decreased as V_f increased. The reduction in plate height of POROS particles at high flow velocities is due to convective enhancement that reduces the overall

Table 3
Split ratio (α) for POROS reversed-phase media. Experimental details are as given under Figs. 4 and 5. D_p is the effective pore diffusivity, α is the split ratio

Media	$D_p \times 10^{11}$ (m^2/s)	$\alpha \times 100$
POROS 20 R1	8.9	0.71
POROS 20 R2	5.2	0.19
Oligo R3	4.2	0.00
POROS 50 R1	5.4	0.34
POROS 50 R2	5.4	0.11

intra-particle mass transfer resistance. If, at high mobile phase velocities, the slope of the Van Deemter curve stabilizes at a constant value substantially greater than zero, then the diffusional resistance in the micro-pores makes a significant contribution to the overall mass transfer resistance of the media. Under these circumstances, a bidisperse model [14,15] will be more suitable for evaluation of the effective pore diffusivity and the split ratio, though at the expense of additional parameters to regress.

5. Conclusions

Predicted values for split ratio and effective pore diffusivity were determined for a highly perfusive supports (POROS 1), perfusive supports with enhanced surface area (POROS 2) and a diffusive support (Oligo R3). Consistent results were obtained for columns packed with POROS HQ 20 and POROS SP 20. The eluite had little effect on the split ratio. This coupled with asymptotic behavior observed for IgG on POROS 20 HQ and POROS 20 SP as well as lysozyme on POROS 20 R1 and POROS 50 R1 verify the assumptions of this model. Media designed to contain the highest fraction of throughpores (POROS 1) exhibited the largest split ratio. Oligo R3 was found to be a purely diffusive support showing no evidence of intra-particle flow. Both the throughpore fraction and split ratios for POROS 2 media were intermediary between POROS 1 and Oligo R3. Regression analysis using a linear model for perfusion chromatography (Eq. 6) successfully distinguished between diffusive and perfusive media.

6. Symbols

a	Characteristic length of the particle (m)
A	Peak area
A_c	Cross sectional area of the column (m^2)
b/a	Asymmetry ratio of the peak
C_{kf}	C term component in Eq. 1; external diffusion (s)
C_{Dp}	C term component in Eq. 1; internal diffusion (s)
C_{kl}	C term component in Eq. 1; adsorption rate (s)
d_m	Diameter of the micro-particle (m)
d_p	Particle diameter (m)
D	Free molecular diffusivity (m^2/s)
D_L	Axial dispersion coefficient (m^2/s)
D_p	Effective pore diffusivity (m^2/s)
D_p^a	Apparent pore diffusivity (m^2/s)
F	Volumetric flow-rate (m^3/s)
h	Reduced HETP, H/d_p
h'	Peak height
H	HETP (m)
H_i	Experimental value of HETP (m)
$\hat{H}_i$	Predicted value of HETP (m)
K	Bed permeability (m^2) or Henry's law constant
K_p	Particle permeability (m^2)
L_o	Length of the adsorption column (m)
N	Column efficiency (plates/m)
Re	Reynolds number, $Re=(d_p\rho V_f)/m$
R_p	Radius of the particle, (m)
t_r	Retention time (s)
V_f	Mobile phase superficial velocity, $V_f=(F/A_c)$ (m/s)
v_p	Intra-particle interstitial velocity (m/s)
α	Volumetric interstitial/intra-particle split ratio
ρ	Mobile phase density (kg/m^3)
λ	Intra-particle Peclet number
ε	Interstitial void fraction of the column
ε_p	Void fraction of the particle
μ	Mean of the residence time distribution
σ^2	Variance of the residence time distribution
τ	Tortuosity factor of the media. $(D_p=D/\tau)$

References

[1] G. Neale, N. Epstein, and W. Nader, Chem. Eng. Sci., 28 (1973) 1865.
[2] A. Nir and L.M. Pismen, Chem. Eng. Sci., 32 (1977) 35.
[3] A.E. Rodrigues, in A. Pethö and R.D. Nobel (Editors), Residence Time Distribution Theory in Chemical Engineering, Verlag Chemie, Weinheim, 1 1982, p. 147.
[4] B.J. Ahn, Docteur-Ingenieur Dissertation, Univ. Techologie de Compiègne, Compiègne (1980).
[5] A.E. Rodrigues, B.J. Ahn and A. Zoulalian, AIChE J., 28(4) (1982) 541.
[6] A.E. Rodrigues, J.M. Órfão and A. Zoulalian, Chem. Eng. Commun., 27 (1984) 327.
[7] A. E, Rodrigues and R.M.Q. Ferreira, AIChE Symp. Ser., 84 (1989) 80.
[8] Z.P. Lu, M.M. Dias, J.C.B. Lopes, G. Carta and A.E. Rodrigues, Ind. Eng. Chem. Res., 32 (1993) 1839.

[9] N.B. Afeyan, N.F. Gordon, I. Mazsaroff, L. Varady, S.P. Fulton, Y.B. Yang and F.E. Regnier, J. Chromatogr., 519 (1990) 1.
[10] N.B. Afeyan, F.E. Regnier and R. Dean Jr. US Pat., 5 019 270 (1991).
[11] N.B. Afeyan, Proceedings of the ISPPP-89 meeting held in Philadelphia, PA, USA, 1989.
[12] A.I. Liapis and M.A. McCoy, J. Chromatogr., 599 (1992) 87.
[13] M.A. McCoy, A.I. Liapis and K.K. Unger, J. Chromatogr., 644 (1993) 1.
[14] M.A. McCoy, Ph.D. Dissertation, University of Missouri-Rolla, Rolla, Missouri (1992).
[15] A.I. Liapis and M.A. McCoy, J. Chromatogr. A, 660 (1994) 85.
[16] A.I. Liapis, Y. Xu, O.K. Crosser and A. Tonga, J. Chromatogr. A, 702 (1995) 45.
[17] A.E. Rodrigues, L. Zuping and J.M. Loureiro, Chem. Eng. Sci., 46 (1991) 2765.
[18] A.E. Rodrigues, A.M.D. Ramos, J.M. Loureiro, M. Diaz and Z.P. Lu, Chem. Eng. Sci., 47 (1992) 4405.
[19] A.E. Rodrigues, J.C. Lopes, Z.P. Lu, J.M. Loureiro and M.M. Dias, J. Chromatogr., 590 (1992) 93.
[20] A.E. Rodrigues, Z.P. Lu, J.M. Loureiro and G. Carta, J. Chromatogr. A, 653 (1993) 189.
[21] G. Carta, M.E. Gregory, D.J. Kirwan and H.A. Massaldi, Sep. Technol., 2 (1992) 62.
[22] A.E. Rodrigues, J.M. Loureiro, C. Chenou and M.R. de la Vega, J. Chromatogr. B, 664 (1995) 233.
[23] E. Kuera, J. Chromatogr., 19 (1965) 237.
[24] P. Schneider and J.M. Smith, AIChE J., 14 (1968) 763.
[25] J.J. Van Deemter, F.J. Zuiderweg and A. Klinkenberg, Chem. Eng. Sci., 5 (1956) 271.
[26] R.B. Bird, W.E. Stewart and E.N. Lightfoot, Transport Phenomena, Wiley, New York, 1960.
[27] D.J. Gunn, Chem. Eng. Sci., 42 (1987) 363.
[28] L.S. Snyder and J. J Kirkland, Introduction to Modern Liquid Chromatography, Wiley, New York, 1979.
[29] H.A. Sorber (Editor), Handbook of Biochemistry, Selected Data for Molecular Biology, CRC Press, Cleveland, 1970.